Journal of Electroanalytical Chemistry 794 (2017) 36–42

Contents lists available at ScienceDirect

Journal of Electroanalytical Chemistry

journal homepage: www.elsevier.com/locate/jelechem

Microwave-assisted synthesis of anatase-TiO_2 nanoparticles with catalytic activity in oxygen reduction

Gema Cabello*, Rogério A. Davoglio*, Ernesto C. Pereira

Departamento de Química, Universidade Federal de São Carlos, 13565-905 São Carlos, SP, Brazil

ARTICLE INFO

Keywords:
Anatase-TiO_2
Microwave-assisted hydrothermal synthesis
Sol-gel
Oxygen reduction reaction
Hydrogen peroxide
Electrocatalysis

ABSTRACT

Anatase titanium dioxide nanoparticles were synthesized via fast microwave-hydrothermal route and they were characterized by BET, SEM, XRD and EIS. The synthesis process took barely 20 s, which means a low sintering time which provides a decrease in the cost and energy required in the synthesis process. Pure anatase colloidal TiO_2 particles were obtained under these synthesis conditions. Particulate TiO_2 films were deposited onto high porous graphite substrates and their catalytic activity toward the oxygen reduction reaction in alkaline media was qualitatively demonstrated by cyclic voltammetry and linear sweep voltammetry. The ORR mechanism showed to follow the two-electron pathway via hydrogen peroxide production and further reduction to water.

1. Introduction

Titanium dioxide is one of the most versatile materials with proved applications in energy generation, degradation of organic pollutants, membranes in solar cells, among others [1], since it is relatively inexpensive, chemically and biologically inert, non-toxic, photostable and easy to produce and to use. Depending on the size, it may show mesoporous structure facilitating reactive species adsorption and, therefore, great efficiency in a wide range of catalytic processes [2]. TiO_2 performance may be influenced by surface area, crystal structure and density of surface hydroxyl groups, and all these parameters may differ with different synthesis methods [3]. Among all, the sol-gel process is the most widely used [3], including its combination with contemporary synthesis methods, such as ultrasonic [3], hydrothermal [4–6], solvothermal [3,7], microwave [8–13] and reverse microemulsions [14–20] methods.

Sol-gel processing displays several advantages over other methods of synthesis such as low cost and operating temperature, high chemical homogeneity and purity [21]. However, sol-gel chemistry also has some significant limitations, as (i) low-crystallinity products are obtained which need further calcination processes at elevated temperatures, which may provoke aggregation and/or particle growth, as well as a breakdown of the mesostructure [22–25]; and (ii) the difficulties in obtaining nanosized particles, since the current technology requires very small sized particles for potential application in, for example, nanoelectronics [19]. In addition, long reaction times are usually needed what may lead to contamination of the products. Microwave heating has been employed in an attempt to minimize the reaction time, since it was previously reported to notably spur several reactions [26,27].

The benefits of microwave dielectric heating, over other conventional synthesis methods, are mainly based on its rapid, uniform and energy efficient heating [28]. It means a reduction in the sintering time and temperature what provides a decrease in the cost and energy required in the synthesis process [8]. As a direct consequence of the decrease in reaction time and temperature, a restriction in the particle growth occurs, as well as an improvement in the uniformity of the product together with the microstructure and higher chemical yield [13,29–34]. Furthermore, metal oxide nanoparticles of small size, with the desired crystallinity and good dispersibility are obtained under microwave-synthesis conditions. No additional stabilizing agents are needed, avoiding the contamination of the nanoparticles with intermediate products, which is of great importance for catalytic processes.

However, traditional reagents and/or synthesis routes have been used in the microwave synthesis, which under microwave irradiation generate even more harmful residues. For this reason, the polyol route has emerged as an alternative green microwave-assisted method, especially for metal oxide nanoparticles [35]. In particular, polyethylene glycol (MW 400, PEG 400) shows interesting properties as a reaction media. PEG 400 is nonvolatile, shows low flammability, is biodegradable, thermally stable and may be used as a co-solvent, since it provides a decrease in the polarity of the solution giving an increase in the solubility of organic molecules and it is water soluble. However, by changing the temperature, rich- and poor-polymer phases may appear, resulting in biphasic aqueous systems [36]. Above all, the most interesting from the point of view of metal oxides synthesis, is that PEG

* Corresponding authors.
E-mail addresses: g.cabello@ufscar.br (G. Cabello), rogeriodavoglio@ufscar.br (R.A. Davoglio).

http://dx.doi.org/10.1016/j.jelechem.2017.04.004
Received 23 January 2017; Received in revised form 28 March 2017; Accepted 3 April 2017
Available online 04 April 2017
1572-6657/

has the ability to form complexes with metal cations due to the high amount of ether groups contained in its polymeric chain, similar to crown ethers [37]. In consequence, PEG of different molecular mass has recently emerged as alternative solvents for chemical synthesis [38,39].

The sulfate esterification reaction of alcohols and sulfuric acid, giving acid alkyl sulfates, has been previously postulated [21,40–43]:

$$ROH + H_2SO_4 \rightleftarrows ROSO_3H + H_2O \quad (1)$$

Sulfate esters have long been used as anionic surfactants in the detergent and dye industries, as well as in the production of alcohols from alkenes [44]. Titanium isopropoxide (TIP), as TiO_2 precursor, will be enclosed inside the micelles forming complexes with the hydrophobic hydrocarbon chain via ether groups; whereas the polar sulfate group will be facing the solution. Micellar reaction avoids the fast reaction of hydrolysis of TIP with water in acidic media, and ensures a homogeneous reaction. This system serves as a reaction medium, improving the selectivity. However, since the species location plays an important role, it is necessary to obtain insight in the species-micelle structure. Micellar synthesis has been successfully applied to perform reaction in which organic solvents have been replaced by aqueous surfactant solutions [45]. Using micelles as nanoreactors for nanoparticles synthesis, it is possible to alter the mechanism, since they may stabilize reagents, intermediates and/or products [46] (and the references therein).

There are many remaining problems concerning the development and real application of low temperature fuel cells and metal–air batteries, concerning the development of cost-effective Pt-free catalysts and the reduction of the cathode over-potential, considering the limited kinetics of the oxygen reduction reaction (ORR) at the cathode. In this way, transition metal oxides have been previously reported to show high activity toward the ORR [47,48] and titanium dioxide remains as a suitable candidate due to its valuable properties mentioned above, and since it is a cost-effective material. The most valuable mechanism, from application point of view, is related to the direct 4-electron reduction pathway from O_2 to H_2O [49]. However, most common mechanisms include a sequence of steps with H_2O_2 as intermediate, leading to a loss in cell potential what could be only reduced by further reducing the peroxide formed. In addition, in alkaline solutions, the reduction of oxygen to superoxide (O_2^-) via 1 electron may also occur, restricting the potential of oxygen reduction even more acutely than peroxide formation [49].

We report the fast synthesis of colloidal anatase, by microwave-hydrothermal method based on a sulfate esterification reaction, and its application to the oxygen reduction reaction. The main objective of this work is the development of a new route of synthesis for a well-known material with good electrocatalytic properties.

2. Experimental section

2.1. Reagents and materials

Titanium isopropoxide (TIP), polyethylene glycol MW 400 (PEG 400) and sulfuric acid (H_2SO_4) were purchased from Aldrich. All reagents were analytical grade and used as received, without further purification. All solutions were prepared using Milli-Q water (specific conductivity of 18.2 MΩ·cm) and deaerated with nitrogen (99%, White Martins) or oxygen (99.5%, Linde).

2.2. Instrumentation

All electrochemical experiments were carried out on an Autolab PGSTAT302 electrochemical workstation (Eco Chemie) in a conventional three-compartment electrochemical glass cell. The working electrode was a high porous graphite electrode containing a particulate film of TiO_2 and the auxiliary electrode was a platinum wire. All potentials are reported versus the saturated calomel electrode (SCE).

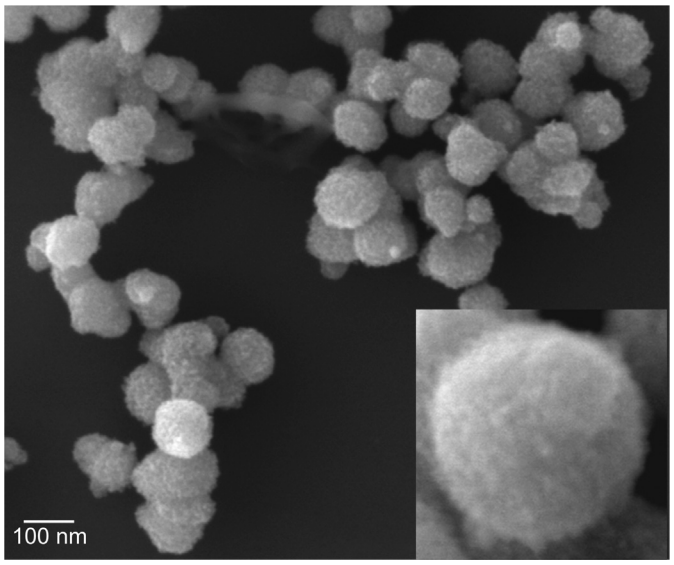

Fig. 1. SEM images of anatase-TiO_2 nanoparticles prepared by microwave-hydrothermal process at 240 °C/10 s.

Table 1
BET surface area calculated from the linear part of the BET plot (P/P_0) = 0.05–0.3.

S_{BET} ($m^2 \cdot g^{-1}$)	Pore volume ($cm^3 \cdot g^{-1}$)	Pore diameter (nm)	Particle size (nm)
83	0.05	2.6	73

Total pore volume, from the volume of N_2 adsorbed at about (P/P_0) = 0.5.

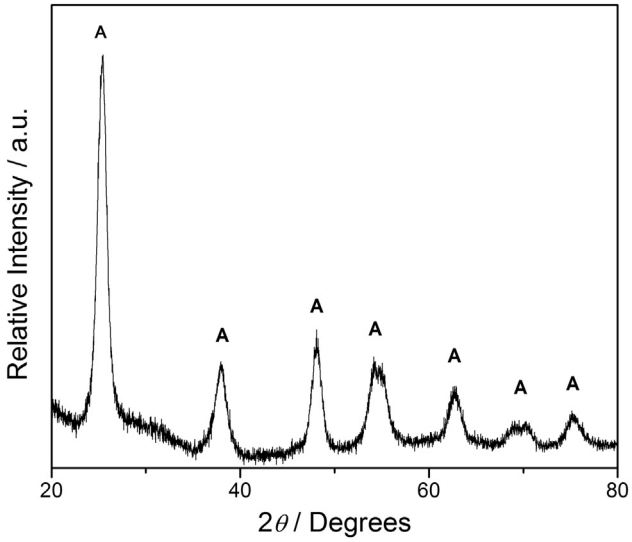

Fig. 2. XRD patterns of anatase-TiO_2 particles synthesized by microwave-hydrothermal process at 240 °C/10 s.

Potentials can be converted to the RHE scale with the following relation: $E(RHE) = E(SCE) + 0.242 + 0.059$ pH. Synthesis of nanoparticles was performed in a microwave reactor Monowave 400 (Anton Paar). The structure of the samples was characterized by the powder X-ray diffraction (XRD), performed on a Shimadzu (XRD-6000) X-ray diffractometer with monochromatized CuKα radiation. The morphologies and crystal structures of as-prepared samples were determined by scanning electron microscopy (SEM, Supra-35 ZEISS FESEM). The surface area of the samples was measured by the Brunauer-Emmett-Teller (BET) method using nitrogen adsorption and desorption isotherms on a Micrometrics ASAP 2020 system. The geometric area of the

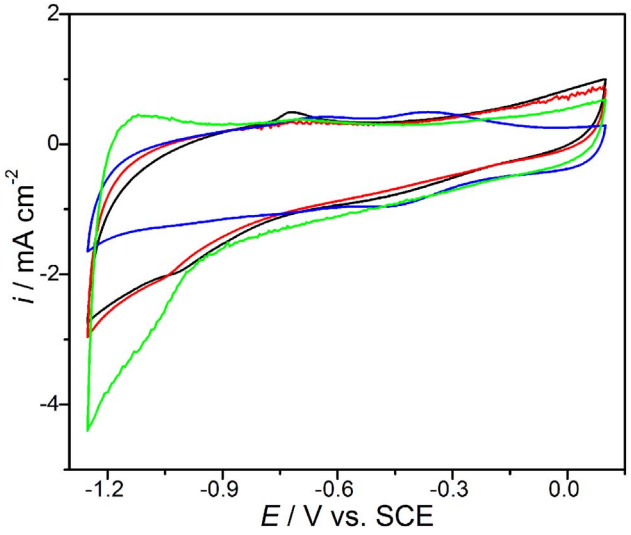

Fig. 3. Cyclic voltammograms of (black) bare graphite and TiO_2-graphite electrodes with different TiO_2 content: (red) 1 mg; (blue) 2 mg; (green) 4 mg, all in an aqueous solution containing 1 M KOH (N_2 saturated), at 50 $mV{\cdot}s^{-1}$. (For interpretation of the references to colour in this figure legend, the reader is referred to the web version of this article.)

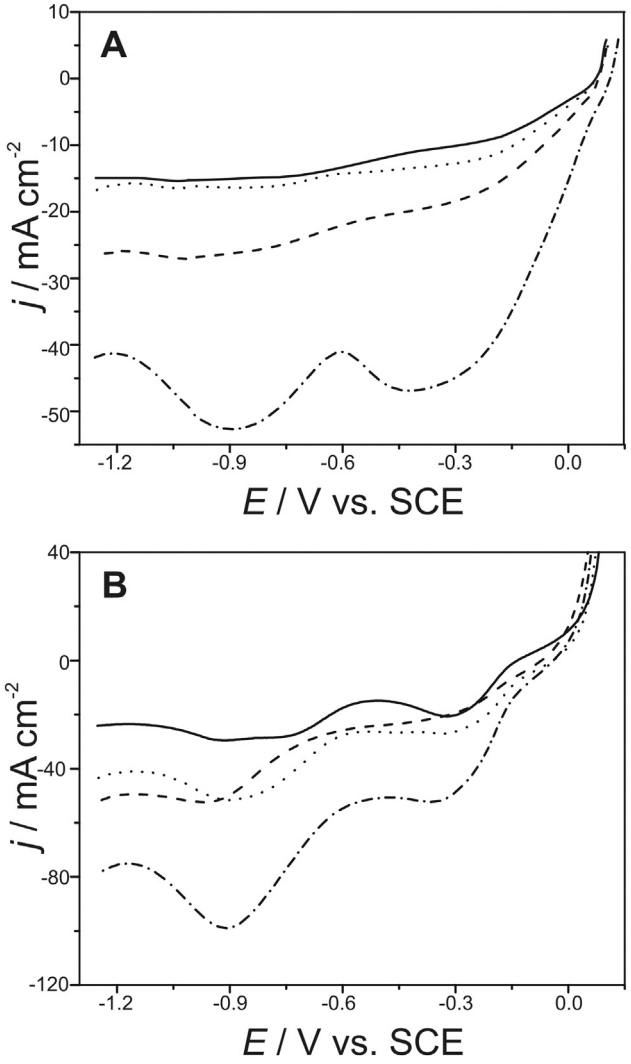

Fig. 4. Polarization curves of (solid line) bare graphite; (dotted line) GT^{I}; (dashed-dotted) GT^{II}; (dashed line) GT^{IV}, in (A) an aqueous solution containing 1 M KOH, O_2 saturated and in (B) an aqueous solution containing 5 mM H_2O_2 and 1 M KOH, O_2 saturated.

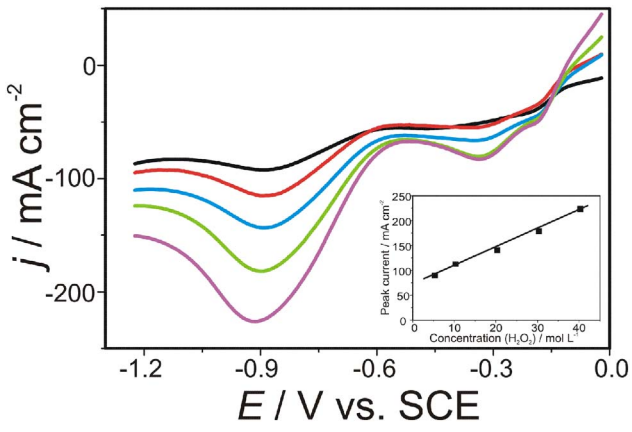

Fig. 5. Polarization curves of GT^{II} electrode in an oxygen-saturated aqueous solution containing (black) 5 mM; (red) 10 mM; (blue) 20 mM; (green) 30 mM; (pink) 40 mM H_2O_2 and 1 M KOH, at 50 $mV{\cdot}s^{-1}$. (For interpretation of the references to colour in this figure legend, the reader is referred to the web version of this article.)

working electrodes was 1.0 cm^2.

2.3. Synthesis of TiO_2 colloidal solution and electrode preparation

Porous TiO_2 nanoparticles were prepared combining a classic sol-gel method with microwave-assisted hydrothermal method. Colloidal solutions were prepared mixing, under vigorous stirring conditions, PEG-400, H_2SO_4, TIP and H_2O (8:6:1 M ratio, respectively, in 10 mL water). A yellowish suspension was obtained after 5 min stirring and it was stable for several days under cool storage conditions. The irreversible hydrolysis of titanium isopropoxide rapidly occurs in the presence of water, leading to the spontaneously formation of titanium oxide. After mixing of the reagents, we did not observe any evidence of particulate precipitates on the reaction vessel, suggesting that a transesterification reaction took place and TIP was encapsulated inside the micelles. Reactants were poured in a glass microwave vessel (30 mL volume) as prepared, and the synthesis was performed under microwave conditions (240 °C for 20 s, 25 bar). Under these conditions, fast nucleation occurred and a colloidal suspension was obtained. It was cooled at room temperature and transferred into a polypropylene centrifuge tube. The suspension was washed and centrifuged several times in water and ethanol and TiO_2 nanoparticles were obtained after removing the supernatant, without calcination. For electrodes preparation, the as-obtained particles were dispersed in DMF, dropped on a high-porous graphite sheet and dried at 300 °C for 24 h. Three different electrodes were prepared containing 1 mg TiO_2 (GT^{I}), 2 mg TiO_2 (GT^{II}) and 4 mg TiO_2 (GT^{IV}).

3. Results and discussion

The morphology and structure of TiO_2 particles were characterized by SEM (Fig. 1). Spherical shaped particles showed an average size of 100 nm diameter and they appeared as aggregates, as a result of the fast reaction rates in microwave synthesis. Particles exhibited roughness surface responsible for the high surface area, confirmed by BET analysis. Specific surface area analysis was performed by BET method. Surface area, specific volume and pore diameter are represented in Table 1. Particles showed relative high surface area, which may be further related to the higher catalytic activity attributed to more accessible reactive sites. Pore size distribution, obtained from BJH method, indicated a narrow distribution with average pore diameter of 2.6 nm. Particles consisted of 0.05 $cm^3{\cdot}g^{-1}$ pore volume, which provides estimated porosity [50] of 34%. The average particle size was estimated in 73 nm, in good agreement with data obtained from SEM analysis. BET analysis suggests high roughness particles containing small pores.

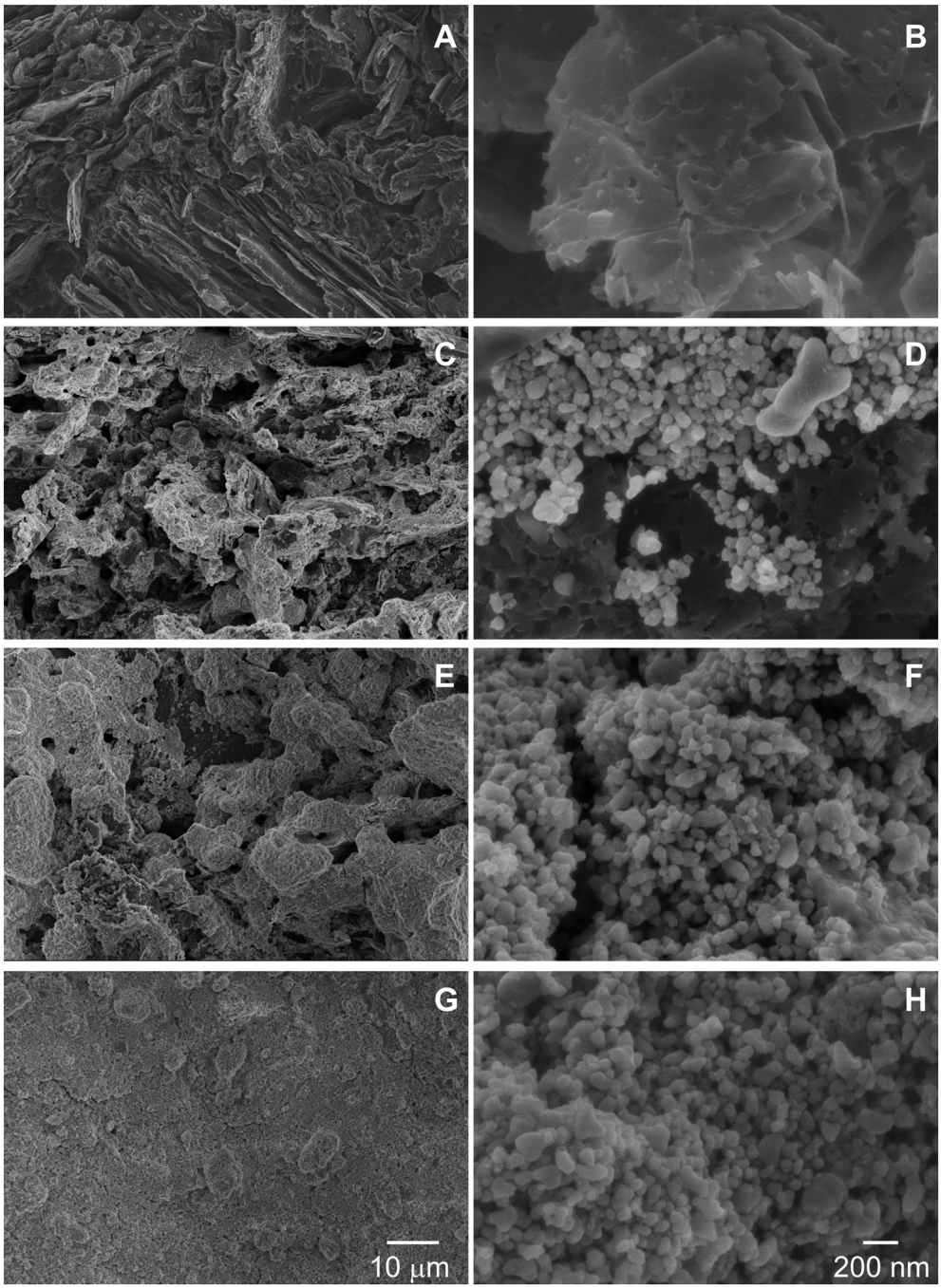

Fig. 6. SEM images of bare graphite (A–B) and TiO_2-graphite electrodes (C–D) GT^I; (E–F) $GT^I I$ and (G–H) GT^{IV}, at different magnifications.

The XRD patterns of the as-synthesized TiO_2 are shown in Fig. 2. The sample showed all characteristic peaks of anatase (JCPDF# 21-1272). Crystalline phase particles containing some defects were obtained by microwave-hydrothermal synthesis route without further calcination.

Graphite electrodes have been previously used as a support for titanium oxide in catalysis [51], mainly due to its high specific surface area and its intrinsic chemical and thermal stability. Fig. 3 shows cyclic voltammograms (CV) of all electrodes performed in an aqueous solution containing 1 M KOH (N_2 saturated), at 50 $mV{\cdot}s^{-1}$. CV of bare graphite electrode (black line) showed typical features with an oxidation peak at ca. − 0.7 V and the corresponding reversible reduction peak at ca. − 1.0 V associated to surface adsorbed species. Graphite may contain surface adsorbed groups as OH, C═O and C—H [52] with reversible electrochemical activity. Addition of TiO_2 nanoparticles strongly affected the electrochemical response of the electrodes, as evidenced by the suppression of the above mentioned reversible oxidation/reduction peaks, what became more reversible since the coverage of the graphite increased. It can also be found, related to the increase deposit of TiO_2 particles, typical feature corresponding to the reduction of electroactive Ti^{4+} [53], at ca. − 1.1 V. The electrochemical profile progressively changed from the bare graphite electrode to the 4 mg TiO_2-graphite electrode. Increasing the titanium oxide content led to a decrease in the graphite electrochemical response and the voltammetric profile approximated to a pure titanium oxide electrode [54].

The electrocatalysts activity was explored by polarization measurements in aqueous solution containing 1 M KOH (O_2 saturated) within a potential range from 0.1 V to − 1.25 V, at 50 $mV{\cdot}s^{-1}$ (Fig. 4). The catalytic activity of carbon materials toward the ORR has been previously reported [55,56], with evidences to enhanced interaction

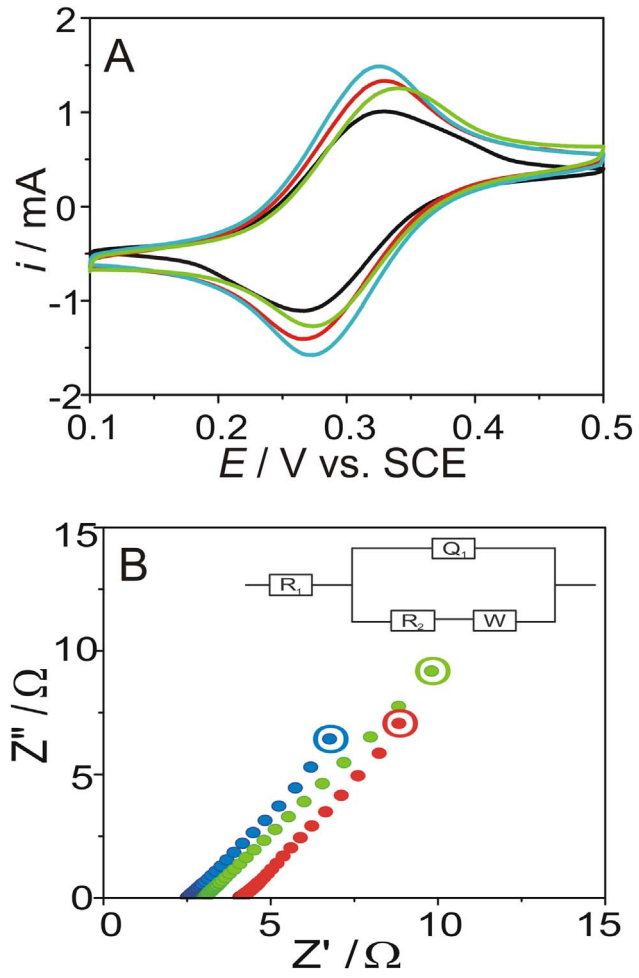

Fig. 7. (A) Cyclic voltammograms of all electrodes, performed at 1 $mV{\cdot}s^{-1}$. (Black) Bare graphite and graphite/TiO_2 electrodes: (red) GT^{I}; (blue) GT^{II}; (green) GT^{IV}. (B) Nyquist plot of (red) GT^{I}, (blue) GT^{I} and (green) GT^{IV} TiO_2-graphite electrodes in 1 M Na_2SO_4 containing 5 mM $Fe(CN)_6^{4-}$/$Fe(CN)_6^{3-}$. Highlighted (O) represents 60 MHz frequency. (For interpretation of the references to colour in this figure legend, the reader is referred to the web version of this article.)

Table 2
Impedance data for graphite/TiO_2 electrodes.

	GT^{I}	GT^{II}	GT^{IV}
R_1 / Ω	4.1	2.5	3.0
Q_1 ($*10^{-1}$) / $\Omega^{-1}{\cdot}sn$	1.6	1.8	1.3
n	0.85	0.86	0.83
R_{ct} / Ω	1.8	3.0	3.7
W ($*10^{-6}$) / $\Omega{\cdot}s^{-1/2}$	1.2	0.39	0.012
χ^2 ($*10^{-5}$)	6.7	9.6	2.0

Experiments were performed in a solution containing 5 mM $Fe(CN)_6^{4-/3-}$.

of O_2 with species at the graphite surface. Depending on the type, graphite can (i) catalyze the ORR via 2-electron pathway, producing H_2O_2 or (ii) further reduced until H_2O formation, and the same reaction mechanism occurs at the TiO_2 surface [56,57]:

$$O_{2(ads)} + e^- \rightarrow O_{2(ads)}^- \quad (2)$$

$$O_{2(ads)}^- + H_2O + 2e^- \rightarrow HO_{2(ads)}^- + OH^- \quad (3)$$

$$HO_2^- + H_2O + 2e^- \rightarrow 3OH^- \quad (4)$$

LSV profiles for all electrodes showed two cathodic irreversible peaks. Bare graphite electrode (Fig. 4A solid line) showed little activity toward the ORR, as expected and the activity did not increase substantially in the case of the electrode containing 1 mg of TiO_2 particles (Fig. 4A dotted line), showing that this amount of TiO_2 was not enough to provoke a larger effect than that of the substrate. On the contrary, double amount of TiO_2 (Fig. 4A dashed-dotted line) led to a markedly increase in the signal exhibiting two well-separated two electrons reduction peaks [58]. The first peak at ca. − 0.3 V can be ascribed as the oxygen reduction via 2 electrons (Eqs. 2 and 3) and the second peak at ca. − 0.9 V as the subsequent reduction to water via 2 electrons (Eq. 4). In the case of the GT^{IV} electrode (Fig. 4A dashed line), cathodic currents were surprisingly lower compared to those obtained for the GT^{II} electrode (Fig. 4A dashed-dotted line). This feature will be explained below.

To correlate the peaks with the reaction mechanism, polarization curves were acquired after the addition of 5 mM H_2O_2, O_2 saturated (Fig. 4B). Two well-defined cathodic peaks were clearly observed and the second peak (ca. − 0.9 V) showed higher peak currents compared to that at ca. − 0.3 V, indicating that corresponds to hydrogen peroxide reduction to water. Again, the electrode containing 2 mg TiO_2 showed higher catalytic activity.

Experiments with successive addition of hydrogen peroxide are represented in Fig. 5. Successive aliquots were added to obtain final concentration of 5, 10, 20, 30 and 40 mM H_2O_2. Results showed a linear increase of the peak current with the hydrogen peroxide concentration (see inset) and that the potential peak progressively shifted to more cathodic potentials. These results confirm the background of the second peak, which can be certainly ascribed to the H_2O_2 reduction reaction.

The catalytic performance of our materials toward the ORR was found to be higher to that of other TiO_2 materials prepared by other methods [58–61]. After geometric area normalization, we obtained current densities up to ten times higher than those shown in literature. We ascribe these high currents to the higher mass of catalytic material and the difficulty of comparing results in the area of materials science.

SEM images of graphite (Fig. 6A–B) and graphite-TiO_2 electrodes, with different TiO_2 content are shown in Fig. 6C–H. Bare graphite shows a high roughness and irregular surface with porous cavities. After functionalization with TiO_2, surface appeared smoother since TiO_2 has filled the graphite pores, forming about a uniform film and the film morphology is strongly influenced by the amount of TiO_2. For electrodes with low TiO_2 content (Fig. 6C–D), barely half of the surface was covered, in good agreement with the results obtained by CV (Fig. 4A), in which the voltammetric profile was similar to that observed in bare graphite. Increasing the TiO_2 content up to 2 mg led to the complete coverage of the graphite surface but not to pore blocking (Fig. 6E–F). On the contrary, for high TiO_2 content, particle accumulation completely saturated graphite pores and a thick film was formed (Fig. 6G–H). SEM analysis supports previous results obtained by CV. Increasing the amount of TiO_2 increased the voltammetric response to the ORR, until the graphite surface is covered to such a degree to impede the electron transfer. A semiconductor particulate thick film substantially covering the graphite surface may behave as an electron-transfer barrier. Therefore, the voltammetric profile for GT^{IV} electrodes is close to that of bare graphite since the electrochemical process preferentially may occur in the graphite face free of titanium oxide barrier.

Electrochemical impedance spectroscopy studies (EIS) were performed to characterize processes at graphite/TiO_2/electrolyte interfaces (Fig. 7B), associated to their respective resistance (R) and capacitance (Q). Measurements were performed in 1 M Na_2SO_4 containing 5 mM $Fe(CN)_6^{4-}$/$Fe(CN)_6^{3-}$, in a frequency range between 60 MHz to 10 KHz and 10 mV (rms), and the corresponding cyclic voltammograms are shown in Fig. 7A. All electrodes showed good reversibility toward redox processes, with a ΔE_p close to 54 mV (at 1 $mV{\cdot}s^{-1}$). Experimental results (from the cathodic peak) were addressed by spectra simulation with an equivalent circuit and a non-linear least squares fitting (NLLS) algorithm [62]. Frequency responses were measured under potentiostatic conditions at 0.25 V (SCE).

In the present case, a Randles equivalent circuit has been used for

the data fitting which is represented in the inset of Fig. 7B. In this equivalent circuit, R_1 represents the ohmic resistance of the electrolyte; Q_1 is the non-ideal capacitance of the electrical double layer (substrate/TiO_2/electrolyte interface), represented by a constant phase element; n is the exponential coefficient of Q_1; R_{tc} is the charge transfer resistance $Fe(CN)_6^{4-}/Fe(CN)_6^{3-}$ reaction; W (Warburg coefficient) is the diffusion coefficient of $Fe(CN)_6^{4-}/Fe(CN)_6^{3-}$ to the electrode surface. The fitting parameters together with adjustment quality coefficient, χ^2, are presented in Table 2. R_{tc} increased with TiO_2 content, what may be ascribed to a decrease in the reaction rate. Such behaviour could also be attributed to an increase of the ohmic drop in the TiO_2 layer. Q_1 corroborates this proposition, since Q_1 increased from GT^I to GT^{II} and diminished from GT^{II} to GT^{IV}. The important decrease in W, from GT^I to GT^{IV}, could be also associated to a decrease in the mass transport through the TiO_2 layer, in concordance with results shown in Fig. 6. Q_1 slightly increased from GT^I to GT^{II}, but decreased in the case of GT^{IV}, which may be attributed to a partial decrease in the surface area (please, see Fig. 6G). EIS analysis supports the results obtained from cyclic voltammetry and further explains the better efficiency of GT^{II} to the ORR.

4. Conclusions

Colloidal TiO_2 nanoparticles were synthesized by microwave-assisted hydrothermal route, based on a sulfate esterification reaction. The synthesis process took barely 20 s, which means a low sintering time which provides a decrease in the cost and energy required in the synthesis process. As a direct consequence of the decrease in reaction time, a restriction in the particle growth occurs, as well as an improvement in the uniformity of the product and higher chemical yield, leading to pure anatase particles with high surface area (without further calcination). It is suggested that microwave-assisted hydrothermal route can provide novel materials for a wider range of applications, including electrochemical ones. In such a way, as an example, we have applied the as-synthesized TiO_2 nanoparticles for the ORR.

Electroactive TiO_2 particulate films were deposited onto the surface of graphite electrodes and investigated for the oxygen reduction reaction in alkaline media. The use of graphite electrodes, as support for TiO_2 catalysts, reduced the limitations of planar electrodes regarding to the diffusion of oxygen to the electrode surface. The ORR mechanism qualitatively showed to follow 2-electrons steps, for oxygen reduction to hydrogen peroxide and further reduction to water. TiO_2 content showed to strongly influence the electrodes activity. Increasing the TiO_2 content led to higher catalytic activity, until the TiO_2 layer was thick enough to provoke a hindrance to charge transfer. The as-prepared electrodes showed good catalytic properties with likely applications in hydrogen peroxide production, fuel cells and metal–air batteries.

Acknowledgment

Conselho Nacional de Desenvolvimento Científico e Tecnológico (CNPq) is gratefully acknowledged for financial support under Research Project BJT-2014/400117/2014-2. GC gratefully acknowledges R. Camargo for his collaboration in the acquisition of the SEM images and for useful discussion and suggestions. São Paulo Research Foundation (FAPESP) is also acknowledged for financial support (grant #2013/07296-2). (GC and RAD contributed equally to this work).

References

[1] U. Diebold, The surface science of titanium dioxide, Surf. Sci. Rep. 48 (2003) 53–229.
[2] D.M. Antonelli, J.Y. Ying, Synthesis of hexagonally packed mesoporous TiO_2 by a modified sol–gel method, Angew. Chem. Int. Ed. Eng. 34 (1995) 2014–2017.
[3] D.P. Macwan, P. Dave, S. Chaturvedi, A review on nano-TiO_2 sol–gel type syntheses and its applications, J. Mater. Sci. 46 (2011) 3669–3686.
[4] M. Grätzel, Sol-gel processed TiO_2 films for photovoltaic applications, J. Sol-Gel Sci. Technol. 22 (2001) 7–13.
[5] A.B. Corradi, F. Bondioli, B. Focher, A.M. Ferrari, C. Grippo, E. Mariani, C. Villa, Conventional and microwave-hydrothermal synthesis of TiO_2 nanopowders, J. Am. Ceram. Soc. 88 (2005) 2639–2641.
[6] S. Komarneni, D. Noh Young, Y. Kim Joo, H. Kim Seok, H. Katsuki, Solvothermal/hydrothermal synthesis of metal oxides and metal powders with and without microwaves, Z. Naturforsh. B (2010) 1033.
[7] R.-C. Xie, J. Shang, Morphological control in solvothermal synthesis of titanium oxide, J. Mater. Sci. 42 (2007) 6583–6589.
[8] J.N. Hart, R. Cervini, Y.B. Cheng, G.P. Simon, L. Spiccia, Formation of anatase TiO_2 by microwave processing, Sol. Energy Mater. Sol. Cells 84 (2004) 135–143.
[9] M. Tsuji, M. Hashimoto, Y. Nishizawa, M. Kubokawa, T. Tsuji, Microwave-assisted synthesis of metallic nanostructures in solution, Chem. Eur. J. 11 (2005) 440–452.
[10] X. Chen, S.S. Mao, Titanium dioxide nanomaterials: synthesis, properties, modifications, and applications, Chem. Rev. 107 (2007) 2891–2959.
[11] P. Zhang, S. Yin, T. Sato, Synthesis of high-activity TiO_2 photocatalyst via environmentally friendly and novel microwave assisted hydrothermal process, Appl. Catal., B 89 (2009) 118–122.
[12] J.M. Szeifert, J.M. Feckl, D. Fattakhova-Rohlfing, Y. Liu, V. Kalousek, J. Rathousky, T. Bein, Ultrasmall titania nanocrystals and their direct assembly into mesoporous structures showing fast lithium insertion, J. Am. Chem. Soc. 132 (2010) 12605–12611.
[13] F. Dufour, S. Cassaignon, O. Durupthy, C. Colbeau-Justin, C. Chanéac, Do TiO_2 nanoparticles really taste better when cooked in a microwave oven? Eur. J. Inorg. Chem. 2012 (2012) 2707–2715.
[14] V. Chhabra, V. Pillai, B.K. Mishra, A. Morrone, D.O. Shah, Synthesis, characterization, and properties of microemulsion-mediated nanophase TiO_2 particles, Langmuir 11 (1995) 3307–3311.
[15] J. Eastoe, B. Warne, Nanoparticle and polymer synthesis in microemulsions, Curr. Opin. Colloid Interface Sci. 1 (1996) 800–805.
[16] Y. Mori, Y. Okastu, Y. Tsujimoto, Titanium dioxide nanoparticles produced in water-in-oil emulsion, J. Nanopart. Res. 3 (2001) 219–225.
[17] M. Andersson, L. Österlund, S. Ljungström, A. Palmqvist, Preparation of nanosize anatase and rutile TiO_2 by hydrothermal treatment of microemulsions and their activity for photocatalytic wet oxidation of phenol, J. Phys. Chem. B 106 (2002) 10674–10679.
[18] V. Uskoković, M. Drofenik, Reverse micelles: inert nano-reactors or physico-chemically active guides of the capped reactions, Adv. Colloid Interf. Sci. 133 (2007) 23–34.
[19] M. Fernández-García, C. Belver, J.C. Hanson, X. Wang, J.A. Rodriguez, Anatase-TiO_2 nanomaterials: analysis of key parameters controlling crystallization, J. Am. Chem. Soc. 129 (2007) 13604–13612.
[20] C.E. Zubieta, J.F.A. Soltero-Martínez, C.V. Luengo, P.C. Schulz, Preparation, characterization and photoactivity of TiO_2 obtained by a reverse microemulsion route, Powder Technol. 212 (2011) 410–417.
[21] C. Han, J. Andersen, V. Likodimos, P. Falaras, J. Linkugel, D.D. Dionysiou, The effect of solvent in the sol–gel synthesis of visible light-activated, sulfur-doped TiO_2 nanostructured porous films for water treatment, Catal. Today 224 (2014) 132–139.
[22] B. O'Regan, M. Gratzel, A low-cost, high-efficiency solar cell based on dye-sensitized colloidal TiO_2 films, Nature 353 (1991) 737–740.
[23] H. Lindström, H. Rensmo, S. Södergren, A. Solbrand, S.-E. Lindquist, Electron transport properties in dye-sensitized nanoporous – nanocrystalline TiO_2 films, J. Phys. Chem. 100 (1996) 3084–3088.
[24] Y. Li, J. Hagen, W. Schaffrath, P. Otschik, D. Haarer, Titanium dioxide films for photovoltaic cells derived from a sol–gel process, Sol. Energy Mater. Sol. Cells 56 (1999) 167–174.
[25] P. Yang, D. Zhao, D.I. Margolese, B.F. Chmelka, G.D. Stucky, Block copolymer templating syntheses of mesoporous metal oxides with large ordering lengths and semicrystalline framework, Chem. Mater. 11 (1999) 2813–2826.
[26] V.K. Saxena, U. Chandra, Microwave synthesis: a physical concept, in: U. Chandra (Ed.), Microwave Heating, InTech, 2011.
[27] V.B. Yu, K.I. Rybakov, V.E. Semenov, High-temperature microwave processing of materials, J. Phys. D. Appl. Phys. 34 (2001) R55.
[28] S. Sayoko, T. Tomoya, K. Takashi, M. Kohsuke, Y. Hiromi, Application of microwave to the synthesis of nanosized metal and alloy catalysts on titanium dioxide supports, J. Phys. Conf. Ser. 165 (2009) 012039.
[29] S.A. Nightingale, D.P. Dunne, H.K. Worner, Sintering and grain growth of 3 mol% yttria zirconia in a microwave field, J. Mater. Sci. 31 (1996) 5039–5043.
[30] Z.-P. Xie, X.-D. Fan, Y. Huang, Accelerated sintering and phase transformation of TiO_2 in microwave radiation, J. Mater. Res. 13 (1998) 3417–3422.
[31] S. Ananthakumar, G. Krishnapriya, A.D. Damodaran, K.G.K. Warrier, Thermal decomposition characteristics of boehmite gels under microwave heating and associated microstructural features, Mater. Lett. 35 (1998) 95–99.
[32] D.K. Agrawal, Microwave processing of ceramics, Curr. Opin. Solid State Mater. Sci. 3 (1998) 480–485.
[33] B.L. Newalkar, J. Olanrewaju, S. Komarneni, Direct synthesis of titanium-substituted mesoporous SBA-15 molecular sieve under microwave – hydrothermal conditions, Chem. Mater. 13 (2001) 552–557.
[34] V.K. Saxena, U. Chandra, Microwave Synthesis: A Physical Concept, (2011).
[35] I. Bilecka, M. Niederberger, Microwave chemistry for inorganic nanomaterials synthesis, Nano 2 (2010) 1358–1374.
[36] J. Chen, S.K. Spear, J.G. Huddleston, R.D. Rogers, Polyethylene glycol and solutions of polyethylene glycol as green reaction media, Green Chem. 7 (2005) 64–82.
[37] G.E. Totten, N.A. Clinton, Poly[ethylene glycol] derivatives as phase transfer catalysts and solvents for organic reactions, J. Macromol. Sci. C Polym. Rev. J. 28

(1988) 293–337.
[38] F.L. Neil, C. Reid, L.G. John, J.K. Donald, Aqueous polyglycol solutions as alternative solvents, Clean Solvents, American Chemical Society, 2002, pp. 208–223.
[39] J. Liang, J. Lv, J.-c. Fan, Z.-c. Shang, Polyethylene glycol as a nonionic liquid solvent for the synthesis of N-alkyl and N-arylimides, Synth. Commun. 39 (2009) 2822–2828.
[40] N.C. Deno, M.S. Newman, Mechanism of sulfation of alcohols1,2, J. Am. Chem. Soc. 72 (1950) 3852–3856.
[41] M.I. Vinnik, I.S. Kislina, A.N. Kitaigorodskii, A.T. Nikitaev, Kinetics and mechanism of formation and hydrolysis of acid methyl sulfate in aqueous solutions of sulfuric acid, Bull. Acad. Sci. USSR 35 (1986) 2447–2453 (Division of chemical science).
[42] E.C. Minerath, M.T. Casale, M.J. Elrod, Kinetics feasibility study of alcohol sulfate esterification reactions in tropospheric aerosols, Environ. Sci. Technol. 42 (2008) 4410–4415.
[43] J. Li, M. Jang, Kinetic study of esterification of sulfuric acid with alcohols in aerosol bulk phase, Atmos. Chem. Phys. Discuss. 13 (2013) 23217–23250.
[44] C.P. Hoiberg, R.O. Mumma, Preparation of sulfate esters. Reactions of various alcohols, phenols, amines, mercaptans, and oximes with sulfuric acid and dicyclohexylcarbodiimide, J. Am. Chem. Soc. 91 (1969) 4273–4278.
[45] J.H.M. Heijnen, V.G.d. Bruijn, L.J.P.v.d. Broeke, J.T.F. Keurentjes, Micellar catalysis as a clean alternative for selective epoxidation reactions, Clean Solvents, American Chemical Society, 2002, pp. 191–207.
[46] S. Ta§cioğlu, Micellar solutions as reaction media, Tetrahedron 52 (1996) 11113–11152.
[47] A. Manthiram, A. Vadivel Murugan, A. Sarkar, T. Muraliganth, Nanostructured electrode materials for electrochemical energy storage and conversion, Energy Environ. Sci. 1 (2008) 621–638.
[48] G. Wu, P. Zelenay, Nanostructured nonprecious metal catalysts for oxygen reduction reaction, Acc. Chem. Res. 46 (2013) 1878–1889.
[49] D.M. Dimarco, Oxygen Reduction on a Graphite Paste and a Catalyst Loaded Graphite Paste Electrode, AA (Ames Lab., IA.), Iowa State University, 1980, p. 170.
[50] J.C. Yu, Yu, Ho, Jiang, Zhang, Effects of F-doping on the photocatalytic activity and microstructures of nanocrystalline TiO_2 powders, Chem. Mater. 14 (2002) 3808–3816.
[51] J.C.M. Silva, R.F.B. De Souza, G.S. Buzzo, E.V. Spinacé, A.O. Neto, M.H.M.T. Assumpção, Effect of the TiO_2 content as support with carbon toward methanol electro-oxidation in alkaline media using platinum nanoparticles as electrocatalysts, Ionics 20 (2014) 1137–1144.
[52] T. Pellenbarg, N. Dementev, R. Jean-Gilles, C. Bessel, E. Borguet, N. Dollahon, R. Giuliano, Detecting and quantifying oxygen functional groups on graphite nanofibers by fluorescence labeling of surface species, Carbon 48 (2010) 4256–4267.
[53] M. Koelsch, S. Cassaignon, J.F. Guillemoles, J.P. Jolivet, Comparison of optical and electrochemical properties of anatase and brookite TiO_2 synthesized by the sol–gel method, Thin Solid Films 403–404 (2002) 312–319.
[54] F.Y. Oliva, L.a.B. Avalle, V.A. Macagno, C.P. De Pauli, Study of human serum albumin-TiO_2 nanocrystalline electrodes interaction by impedance electrochemical spectroscopy, Biophys. Chem. 91 (2001) 141–155.
[55] E. Yeager, Dioxygen electrocatalysis: mechanisms in relation to catalyst structure, J. Mol. Catal. 38 (1986) 5–25.
[56] C. Song, J. Zhang, Electrocatalytic oxygen reduction reaction, in: J. Zhang (Ed.), PEM Fuel Cell Electrocatalysts and Catalyst Layers: Fundamentals and Applications, Springer London, London, 2008, pp. 89–134.
[57] C. Paliteiro, A. Hamnett, J.B. Goodenough, The electroreduction of oxygen on pyrolytic graphite, J. Electroanal. Chem. Interfacial Electrochem. 233 (1987) 147–159.
[58] M.A. Ghanem, A.M. Al-Mayouf, M.N. Shaddad, F. Marken, Selective formation of hydrogen peroxide by oxygen reduction on TiO_2 nanotubes in alkaline media, Electrochim. Acta 174 (2015) 557–562.
[59] K. Jukk, N. Kongi, A. Tarre, A. Rosental, A.B. Treshchalov, J. Kozlova, P. Ritslaid, L. Matisen, V. Sammelselg, K. Tammeveski, Electrochemical oxygen reduction behaviour of platinum nanoparticles supported on multi-walled carbon nanotube/titanium dioxide composites, J. Electroanal. Chem. 735 (2014) 68–76.
[60] V.B. Baez, J.E. Graves, D. Pletcher, The reduction of oxygen on titanium oxide electrodes, J. Electroanal. Chem. 340 (1992) 273–286.
[61] B. Ruiz-Camacho, O. Martínez-Álvarez, H.H. Rodríguez-Santoyo, V. Granados-Alejo, Pt/C and Pt/TiO_2–C electrocatalysts prepared by chemical vapor deposition with high tolerance to alcohols in oxygen reduction reaction, J. Electroanal. Chem. 725 (2014) 19–24.
[62] B.A. Boukamp, A Nonlinear Least Squares Fit procedure for analysis of immittance data of electrochemical systems, Solid State Ionics 20 (1986) 31–44.